Universal behavior of quantum walks with long-range steps

Oliver Mülken,* Volker Pernice, and Alexander Blumen
Theoretische Polymerphysik, Universität Freiburg, Hermann-Herder-Straße 3, 79104 Freiburg, Germany
(Received 23 November 2007; published 15 February 2008)

Continuous-time quantum walks with long-range steps $R^{-\gamma}$ (R being the distance between sites) on a discrete line behave in similar ways for all $\gamma \geq 2$. This is in contrast to classical random walks, which for $\gamma > 3$ belong to a different universality class than for $\gamma \leq 3$. We show that the average probabilities to be at the initial site after time t as well as the mean square displacements are of the same functional form for quantum walks with $\gamma=2$, 4, and with nearest neighbor steps. We interpolate this result to arbitrary $\gamma \geq 2$.

DOI: 10.1103/PhysRevE.77.021117 PACS number(s): 05.60.Gg, 03.67.−a, 05.60.Cd, 71.35.−y

One-dimensional models are not only prime toys for theoretical physicists but also allow for deep physical insights. For instance, in solid state physics lattice models describe the behavior of metals quite accurately [1,2]. Over the years these models have been refined and augmented to address different phenomena, such as the dynamics of atoms in optical lattices and the Anderson localization in systems with energetic disorder [3]. Classical one-dimensional models allow to address various aspects of normal and anomalous diffusion [4].

The simplest model describing a particle moving on a regular structure assumes only jumps from one position j to its nearest neighbors (NN) $j \pm 1$. The tight-binding approximation for such systems is equivalent to the so-called continuous-time quantum walks (CTQW), which model quantum dynamics of excitations on networks [5–7]. Related discrete-time models are (coined) quantum random walks [8] and, more abstract, quantum baker maps [9], both of which have dynamical properties similar to CTQW. Recently, there have been several experimental proposals addressing CTQW in various types of systems, ranging from microwave cavities [10], waveguide arrays [11], atoms in optical lattices [12,13], or structured clouds of Rydberg atoms [14]. A large class of these systems do not show NN steps. Consider, for instance, a chain of clouds of Rydberg atoms where each cloud can contain only one excitable atom due to the dipole blockade [14,15]. The excited atoms of different clouds interact via long-range couplings decaying as R^{-3}, where R is the distance between different clouds.

The dynamics of classical excitations can be efficiently described by continuous-time random walks (CTRW) [16]. There it was shown that CTRW in one dimension with step lengths decaying as $R^{-\gamma}$ belong only to the same universality class if $\gamma > 3$. Those CTRW show normal diffusion, whereas CTRW with $\gamma < 3$ show anomalous diffusion as, e.g., Lévy flights. The reason is that the for $\gamma < 3$ the second moment of the step-length distribution $\langle R^2 \rangle$ diverges [14,17].

In the following we will consider in one dimension the dependence of the CTQW dynamics of excitations on the range of the step length. We restrict ourselves to the extensive cases, i.e., we explicitly exclude ultra-long-range interactions, where the exponent γ of the decay of the step length is smaller than the dimension ($\gamma < d$, $\gamma = d$ is the marginal case); thus we take here $\gamma \geq 2$. The effect of ultra-long-range interactions on the thermodynamics and dynamics of regular one-dimensional lattices has been studied numerically before [18].

Our analysis is based on the density of states (DOS) of the corresponding Hamiltonian. The DOS contains the essential information about the system and allows to calculate various dynamical quantities, such as the probability to be at time t at the initially excited site.

The coherent dynamics of single excitations on a graph of connected two-level systems (nodes) is modeled by CTQW, which follows by identifying the Hamiltonian $\mathbf{H}$ of the system with the CTRW transfer matrix $\mathbf{T}$, i.e., $\mathbf{H}=-\mathbf{T}$; see, e.g. [5,6] (we will set $\hbar \equiv 1$ in the following). For NN step lengths and identical transfer rates, $\mathbf{T}$ is related to the connectivity matrix $\mathbf{A}$ of the graph by $\mathbf{T}=-\mathbf{A}$. In the following, we will consider one-dimensional networks with periodic boundary conditions (i.e., a discrete ring). Here, when the interactions go as $R^{-\gamma}$, with $R=|k-j|$ being the (on the ring minimal) distance between two nodes j and k, the Hamiltonian has the following structure:

$$\mathbf{H}_\gamma = \sum_{n=1}^{N} \sum_{R=1}^{R_{\max}} R^{-\gamma} (2|n\rangle\langle n| - |n-R\rangle\langle n| - |n+R\rangle\langle n|), \quad (1)$$

where $R_{\max}$ is a cutoff for finite systems. Note that in the infinite system limit we first take $N \to \infty$ before also taking $R_{\max} \to \infty$. For the cases considered here, namely $\gamma \geq 2$ and N of the order of a few hundred nodes, a reasonable cutoff is $R_{\max}=N/2$, which is also the largest distance between two nodes on the discrete ring. In this way, to each pair of sites a single (minimal) distance and a unique interaction is assigned.

The states $|j\rangle$ associated with excitations localized at the nodes j ($j=1,\ldots,N$) form a complete, orthonormal basis set of the whole accessible Hilbert space, i.e., $\langle k|j\rangle = \delta_{kj}$ and $\Sigma_k |k\rangle\langle k| = \mathbf{1}$. In general, the transition amplitudes from state $|j\rangle$ to state $|k\rangle$ during t and the corresponding probabilities read $\alpha_{kj}^{(\gamma)}(t) \equiv \langle k|\exp(-i\mathbf{H}_\gamma t)|j\rangle$ and $\pi_{kj}^{(\gamma)}(t) \equiv |\alpha_{kj}^{(\gamma)}(t)|^2$, respectively. In the classical CTRW case the transition probabilities obey a master equation and can be expressed as $p_{kj}^{(\gamma)}(t) = \langle k|\exp(\mathbf{T}_\gamma t)|j\rangle$ [5,6].

*muelken@physik.uni-freiburg.de

For all γ, the time independent Schrödinger equation $\mathbf{H}_\gamma|\Phi_\theta\rangle = E_\gamma(\theta)|\Phi_\theta\rangle$ is diagonalized by Bloch states $|\Phi_\theta\rangle = N^{-1/2}\Sigma_{j=1}^{N}\exp(i\theta j)|j\rangle$. One obtains the eigenvalues

$$E_\gamma(\theta) = \sum_{R=1}^{R_{\max}} R^{-\gamma}[2 - 2\cos(\theta R)]. \tag{2}$$

In the limit $N \to \infty$ the θ values are quasicontinuous. Then, the DOS $\rho_\gamma(E)$ is obtained by inverting Eq. (2) and taking the derivative with respect to E_γ. In the NN case ($\gamma = \infty$) only the first term in Eq. (2), $R=1$, contributes. From this we get the known DOS $\rho_\infty(E) = (\pi\sqrt{4E - E^2})^{-1}$. For $\gamma = 2$ we can approximate the sum by letting $R_{\max} \to \infty$, which yields $E_2(\theta) = \pi\theta - \theta^2/2$ (see Eq. 1.443.3 of [19]). By inverting this and assuming θ to be continuous one obtains $\rho_2(E) = (\pi\sqrt{2}\sqrt{\pi^2/2 - E})^{-1}$. In the intermediate range we have an analytic solution for $\gamma = 4$, namely we have $E_4(\theta) = \theta^4/24 - \pi\theta^3/6 + \pi^2\theta^2/6$ (see Eq. 1.443.6 of [19]), which yields [20] $\rho_4(E) = [2\pi(2/3)^{1/4}\sqrt{E(\pi^2/\sqrt{24}) - E^{3/2}}]^{-1}$.

In order to interpolate between $\rho_2(E)$ and $\rho_\infty(E)$ to arbitrary values of $\gamma \in [2, \infty]$ we assume the following general form for the DOS:

$$\rho_\gamma(E) \sim [\sqrt{c_\gamma E^\alpha - E^\beta}]^{-1} \tag{3}$$

with $\alpha \in [0,1]$ and $\beta \in [1,2]$; c_γ is a constant related to the maximal energy, $c_\gamma \equiv (E_{\gamma,\max})^{\beta-\alpha}$. Thus, for $\gamma = 2$: $\alpha = 0$ and $\beta = 1$ ($c_2 = \pi^2/2$); for $\gamma = 4$: $\alpha = 1$ and $\beta = 3/2$ ($c_4 = \pi^2/\sqrt{24}$); for NN walks: $\alpha = 1$ and $\beta = 2$ ($c_\infty = 4$). For small E, i.e., close to the band edge $\theta = 0$, Eq. (3) can be approximated by

$$\rho_\gamma(E) \sim \begin{cases} E^{-1/2} & \alpha = 1 (\gamma > 3), \\ E^{-\alpha/2} & \alpha < 1 (2 \le \gamma \le 3), \end{cases} \tag{4}$$

from which we observe the distinction between γ values larger and smaller than three. This is in line with previous studies [21], in which the DOS goes as $\rho(E) \sim E^\nu$, where $\nu = -1/2$ for $\gamma > 3$ and $\nu = -(\gamma-2)/(\gamma-1)$ for $2 \le \gamma < 3$. For $E \approx E_{\max}$, i.e., close to the band edge $\theta = \pi$, it is straightforward to show that $\rho(E) \sim (E_{\max} - E)^{-1/2}$ for all $\gamma \ge 2$. Starting from the two limiting cases $\gamma = 2$ and $\gamma = \infty$ and supported by the $\gamma = 4$ case, Eq. (3) appears as a natural candidate for a generalized DOS.

Figure 1 shows a comparison of the DOS obtained from the numerical diagonalization of $\mathbf{H}_\gamma$ for $N = 10\,000$ with $\gamma = 2$, 3, 4, and ∞ (solid black curves) with the exact expressions for $\rho_2(E)$, $\rho_4(E)$, and $\rho_\infty(E)$, see above, as well as a fit for $\rho_3(E)$. The values of α and β, extracted from fits to the numerical DOS for various values of γ, are given in the inset of Fig. 1. Clearly, for $\gamma \ge 4$ we have $\alpha = 1$, while $\beta \in]1,2[$. For $\gamma = 2$, the values of α and β drop to $\alpha = 0$ and $\beta = 1$, respectively.

CTRW with step widths distributed according to R^γ belong to the same universality class for $\gamma > 3$, the mean square displacement (MSD) going as $\langle R^2 \rangle \sim t$, i.e., showing normal diffusion; see, e.g. [16]. For $\gamma \le 3$ the second moment of the distribution diverges, which leads to a MSD showing anomalous diffusion.

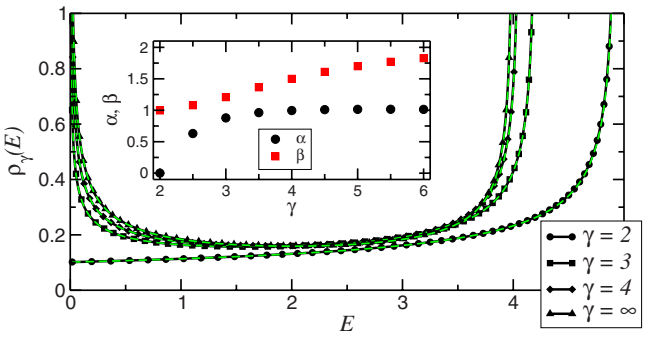

FIG. 1. (Color online) Density of states for a discrete ring with $N = 10\,000$ nodes with hopping parameters $\gamma = 2$, 3, 4, and ∞ (solid black curves with symbols), obtained by numerically diagonalizing $\mathbf{H}_\gamma$. The dashed green curves show the analytic expressions for $\rho_2(E)$, $\rho_4(E)$, and $\rho_\infty(E)$ as well as the fit for $\rho_3(E)$ [Eq. (3)] given in the text. The inset shows the exponents α and β obtained by fitting the DOS for different values of γ to Eq. (3).

Another way to see this is using the *average* probability to be at the initial site at time t, $\bar{p}_\gamma(t)$. Classically one has a simple expression for $\bar{p}_\gamma(t)$ [22,23],

$$\bar{p}_\gamma(t) \equiv \frac{1}{N}\sum_{j=1}^{N} p_{j,j}^{(\gamma)}(t) = \frac{1}{N}\sum_{\theta} \exp[-E_\gamma(\theta)t], \tag{5}$$

which depends only on the eigenvalues but *not* on the eigenvectors. In the quantum case, the corresponding expression is $\bar{\pi}_\gamma(t) \equiv (1/N)\Sigma_{j=1}^{N}\pi_{j,j}^{(\gamma)}(t)$. For the discrete ring, we get

$$\bar{\pi}_\gamma(t) = |\bar{\alpha}_\gamma(t)|^2 = \left|\frac{1}{N}\sum_{\theta}\exp[-iE_\gamma(\theta)t]\right|^2, \tag{6}$$

which also depends only on the eigenvalues. Note that for more complex networks the right-hand side of Eq. (6) is only a lower bound to $\bar{\pi}_\gamma(t)$ [24]. In the continuum limit, Eqs. (5) and (6) can be written as

$$\bar{p}_\gamma(t) = \int dE\, \rho_\gamma(E)\exp(-Et), \tag{7}$$

$$\bar{\pi}_\gamma(t) = \left|\int dE\, \rho_\gamma(E)\exp(-iEt)\right|^2. \tag{8}$$

Having the DOS at hand the integrals in Eqs. (7) and (8) can be calculated—at least asymptotically—for large t. In the classical case Eq. (7) will be dominated by small values of E when t becomes large; see Eq. (4). From the DOS we obtain

$$\bar{p}_\gamma(t) \sim \begin{cases} t^{-1/2}, & \alpha = 1, \\ t^{\alpha/2-1}, & \alpha < 1. \end{cases} \tag{9}$$

Quantum mechanically, some care is in order. Here, the assumption that $\bar{\pi}_\infty(t)$ will be dominated by small values of E for large t is not applicable, due to the oscillating exponential in Eq. (8). For the NN case we know that $\bar{\pi}_\infty(t) \sim t^{-1}$; see, for instance [24]. Considering now the other limiting case $\gamma = 2$, we have

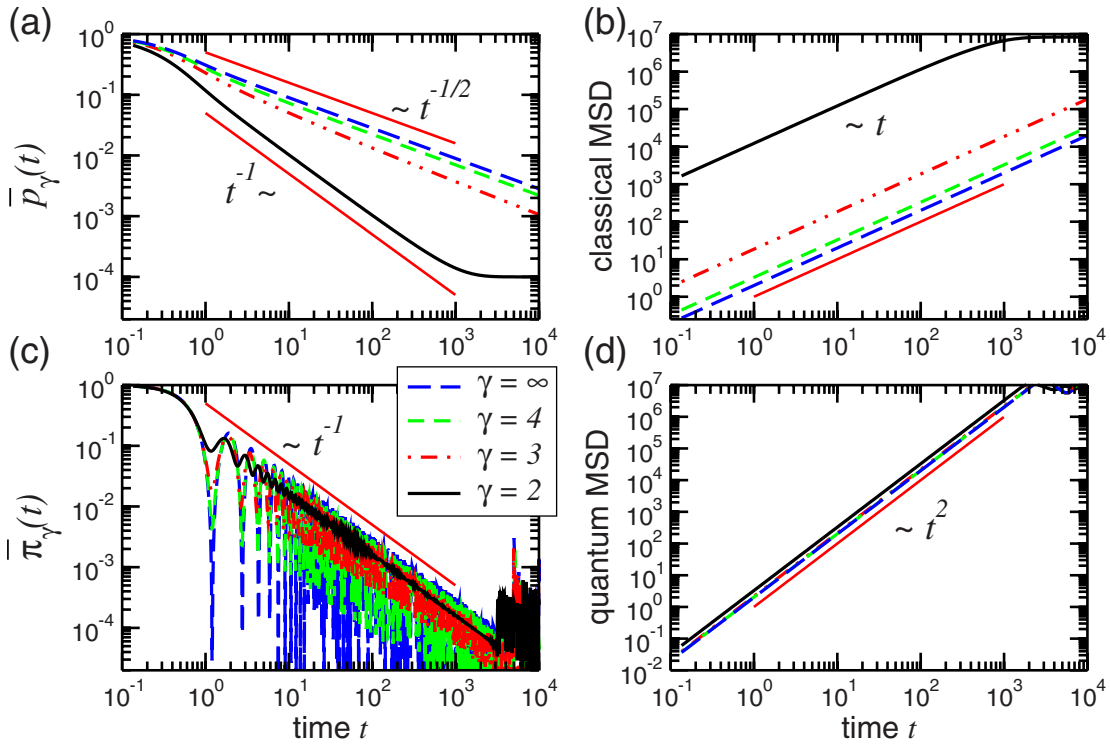

FIG. 2. (Color online) (a) Classical $\bar{p}_\gamma(t)$ and (b) corresponding MSD; (c) quantum mechanical $\bar{\pi}_\gamma(t)$ and (d) corresponding MSD (right) for a discrete ring with $N=10\,000$ nodes with $\gamma=2$, 3, 4, and ∞.

$$\bar{\pi}_2(t) = \left| \int_0^{\pi^2/2} dE \frac{\exp(-iEt)}{\pi\sqrt{2}\sqrt{\pi^2/2 - E}} \right|^2 \sim t^{-1}. \tag{10}$$

Note that for $t \gg 1$, Eq. (10) approaches $\bar{\pi}_2(t) \approx (2\pi t)^{-1}$. Thus the dependence of $\bar{\pi}_2(t)$ on t is the same as for $\bar{\pi}_\infty(t)$. This suggests that for all one-dimensional lattices with extensive ($\gamma \geq 2$) interactions the long time dynamics of the excitations is similar, no matter how long- or short-range the step lengths are. This is in contrast to the classical case, where only CTRW with $\gamma > 3$ belong to the same universality class.

To test this we calculated numerically for a discrete ring of $N=10\,000$ nodes $\bar{p}_\gamma(t)$ and $\bar{\pi}_\gamma(t)$ for different γ; the results are shown in Fig. 2. Clearly, $\bar{p}_\gamma(t)$ changes when increasing the step width from NN steps ($\gamma=\infty$) to long-range steps distributed as R^{-2} ($\gamma=2$); see Fig. 2(a). While $\bar{p}_\gamma(t)$ for $\gamma > 3$ decays as $t^{-1/2}$, the power law changes to t^{-1} for $\gamma=2$. In contrast, the decay of the maxima of the quantum return probability $\bar{\pi}_\gamma(t)$ follows t^{-1} for all γ; see Fig. 2(c). Long-range steps lead only to a damping of the oscillations and to an earlier interference once the excitation has propagated half around the ring.

The classical and quantum MSD corroborate these findings; see Figs. 2(b) and 2(d). Now, the MSD for CTRW-CTQW on the discrete ring with initial site j are given by

$$\langle R_\gamma^2(t)\rangle_{\mathrm{cl;qm}} = \frac{1}{N}\sum_{k=1}^{N} |k-j|^2 \mathcal{P}_{k,j}^{(\gamma)}(t), \tag{11}$$

where $\mathcal{P}_{k,j}^{(\gamma)}(t) = p_{k,j}^{(\gamma)}(t)$ for CTRW and $\mathcal{P}_{k,j}^{(\gamma)}(t) = \pi_{k,j}^{(\gamma)}(t)$ for CTQW. Now, decreasing γ has huge effects on the classical MSD. For $2 \leq \gamma < 3$ the MSD starts to diverge, which in the case of finite networks is reflected in the fact that the MSD is of the order of N already for very short times. Increasing γ to values larger than 3 leads to the expected diffusive behavior $\langle R_\gamma^2(t)\rangle_{\mathrm{cl}} \sim t$ for all $\gamma > 3$. The quantum MSD, on the other hand, do not diverge for all γ values considered here. All step lengths lead to the same qualitative behavior, $\langle R_\gamma^2(t)\rangle_{\mathrm{qm}} \sim t^2$.

Figure 2 also shows that the MSD can be related to $\bar{p}_\gamma(t)$ and $\bar{\pi}_\gamma(t)$ through

$$\langle R_\gamma^2(t)\rangle_{\mathrm{cl;qm}} \sim \begin{cases} [\bar{p}_\gamma(t)]^{-2} \\ [\bar{\pi}_\gamma(t)]^{-2} \end{cases} \tag{12}$$

for $\gamma > 3$ in the classical and $\gamma \geq 2$ in the quantal case. This generalizes previous (classical) results, obtained for regular networks with NN-steps [22], to the quantum case and to long-range steps.

We can now underline our results by analytically evaluating $\bar{\pi}_\gamma(t)$ [Eq. (6)] using the stationary phase approximation (SPA) [25]. We expect in general $E_\gamma(\theta)$ to be a smooth real-valued function on the interval $\theta \in [0, 2\pi[$. For large N, we write $\bar{\alpha}_\gamma(t)$ [Eq. (6)] in the integral form

$$\bar{\alpha}_\gamma(t) = \frac{1}{2\pi}\int_0^{2\pi} d\theta \exp[iE_\gamma(\theta)t].$$

The SPA asserts now that the main contribution to this integral comes from those points where $E_\gamma(\theta)$ is stationary $[dE_\gamma(\theta)/d\theta \equiv E'_\gamma(\theta) = 0]$. If there is only one point θ_0 for

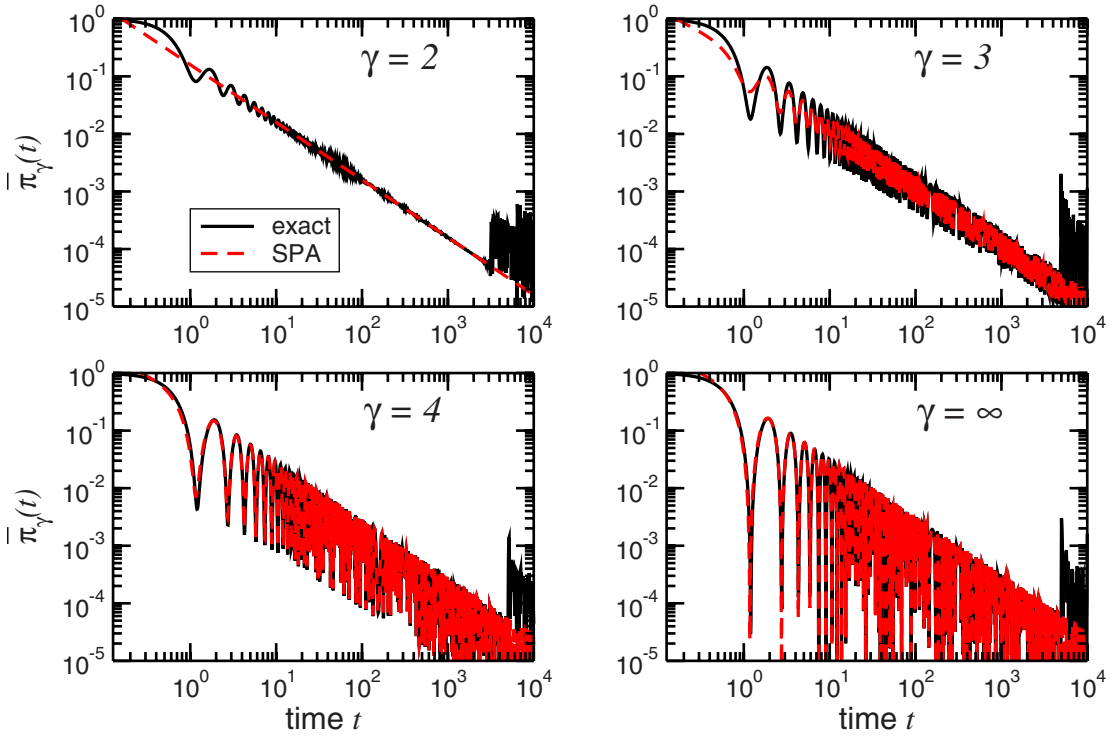

FIG. 3. (Color online) Comparison of $\bar{\pi}_\gamma(t)$ obtained from exact diagonalization (solid black curves) and the SPA (dashed red curves) for $\gamma=2$, 3, 4, and ∞.

which $E'_\gamma(\theta_0)=0$ and $d^2E_\gamma(\theta)/d\theta^2|_{\theta_0}\equiv E''_\gamma(\theta_0)\neq 0$ one gets (see [25])

$$\bar{\alpha}_\gamma(t)\approx\frac{1}{\sqrt{2\pi t|E''_\gamma(\theta_0)|}}\exp\left(i\left\{tE_\gamma(\theta_0)+\frac{\pi}{4}\,\mathrm{sgn}[E''_\gamma(\theta_0)]\right\}\right), \tag{13}$$

such that

$$\bar{\pi}_\gamma(t)=|\bar{\alpha}_\gamma(t)|^2\approx\frac{1}{2\pi t|E''_\gamma(\theta_0)|}\sim t^{-1}. \tag{14}$$

For the infinite one-dimensional regular network [see Eq. (2), where $N\to\infty$ and $R_{\max}\to\infty$] and for $\gamma=2$, $E_2(\theta)$ (see above) has only one stationary point in $\theta\in[0,2\pi[$, namely $\theta_0=\pi$. Then $E_2(\pi)=\pi^2/2$ and $E''_2(\pi)=-1$, leading to $\bar{\pi}_2(t)\approx(2\pi t)^{-1}$, which does not show any oscillations and coincides with the long time limit of Eq. (10).

For $\gamma>2$, $E_\gamma(\theta)$ [see Eq. (2)] has two stationary points in the interval $\theta\in[0,2\pi[$, namely $\theta_0=0$ and $\theta_0=\pi$. Then $\bar{\alpha}_\gamma(t)$ is approximately given by the sum of the contributions [each being of the form given in Eq. (13)] of the two stationary points. One easily verifies from $E''_\gamma(\theta)=2\Sigma_R\cos(\theta R)/R^{\gamma-2}$ that $\mathrm{sgn}[E''_\gamma(0)]=1$ and $\mathrm{sgn}[E''_\gamma(\pi)]=-1$. Consequently, it follows that $\bar{\pi}_\gamma(t)\sim t^{-1}$. The results for the infinite system and arbitrary $\gamma>2$ are readily obtained: For $\theta_0=0$ we have $E_\gamma(0)=0$ for all γ and $E''_\gamma(0)=2\zeta(\gamma-2)$, where $\zeta(\gamma)\equiv\Sigma_{R=1}^{\infty}R^{-\gamma}$ is the Riemann zeta function, Eq. 23.2.1 of [20]. For $\theta_0=\pi$ we get $E_\gamma(\pi)=E_{\gamma,\max}$ and $E''_\gamma(\pi)=2\eta(\gamma-2)=(2-2^{4-\gamma})\zeta(\gamma-2)$, where $\eta(\gamma)\equiv\Sigma_{R=1}^{\infty}(-1)^{R-1}R^{-\gamma}$, Eq. 23.2.19 of [20]. Hence

$$\bar{\pi}_\gamma(t)\approx\frac{1}{4\pi t}\left\{\frac{1}{|\zeta(\gamma-2)|}+\frac{1}{|\eta(\gamma-2)|}-\frac{2\cos[tE_\gamma(\pi)+\pi/2]}{\sqrt{|\zeta(\gamma-2)\eta(\gamma-2)|}}\right\}. \tag{15}$$

For $\gamma=3$, this yields $\bar{\pi}_3(t)\approx[2\pi\ln(2)t]^{-1}$, which also does not show any oscillations. Comparing Eq. (15) for $\gamma=\infty$ to the long-time behavior of the exact solution [24], we have $\bar{\pi}_\infty(t)\approx[2-2\cos(4t+\pi/2)]/(2\pi t)=\sin^2(2t+\pi/4)/(\pi t)$, which is exactly the asymptotic expansion of $\bar{\pi}_\infty(t)=|J_0(2t)|^2\approx\sin^2(2t+\pi/4)/(\pi t)$, where $J_m(2t)$ is the Bessel function of the first kind [20,24].

Figure 3 shows comparisons of $\bar{\pi}_\gamma(t)$ obtained from the exact diagonalization of $\mathbf{H}_\gamma$ (solid black curves) to the SPA (dashed red curves). Clearly, the oscillations decrease with decreasing γ. For $\gamma=2$ and large t, the oscillations of the exact $\bar{\pi}_2(t)$ have practically vanished and $\bar{\pi}_2(t)\approx(2\pi t)^{-1}$. The SPA for $\gamma=3$ still shows oscillations because $E''_\gamma(0)<\infty$. Increasing γ further leads to an even better agreement of the SPA with the numerically evaluated decay.

In conclusion, we have analyzed the quantum dynamics of excitations on discrete rings under long-range step lengths, distributed according to $R^{-\gamma}$. For specific cases, we calculated the DOS analytically and interpolated to arbitrary step length ranges. The analytically obtained DOS enabled

us to analytically calculate the average probability to be at the initial site at t, which we related to the MSD at time t. The classical MSD show that only CTRW with $\gamma > 3$ belong to the same universality class, displaying normal diffusion. In contrast, the quantal MSD increase as t^2 for *all* extensive cases, $\gamma \geq 2$. Analytic calculations of the probability to be at the initial node within the stationary phase approximations confirm these findings.

Support from the Deutsche Forschungsgemeinschaft (DFG) and the Fonds der Chemischen Industrie is gratefully acknowledged.

[1] J. M. Ziman, *Principles of the Theory of Solids* (Cambridge University Press, Cambridge, England, 1972).
[2] N. W. Ashcroft and N. D. Mermin, *Solid State Physics* (Saunders College Publishing, Philadelphia, 1976).
[3] P. W. Anderson, Phys. Rev. **109**, 1492 (1958).
[4] R. Metzler and J. Klafter, Phys. Rep. **339**, 1 (2000).
[5] E. Farhi and S. Gutmann, Phys. Rev. A **58**, 915 (1998).
[6] O. Mülken and A. Blumen, Phys. Rev. E **71**, 016101 (2005).
[7] S. Bose, Phys. Rev. Lett. **91**, 207901 (2003); M. Christandl, N. Datta, A. Ekert, and A. J. Landahl, *ibid.* **92**, 187902 (2004); D. Burgarth, Ph.D. thesis, University College London, 2006.
[8] Y. Aharonov, L. Davidovich, and N. Zagury, Phys. Rev. A **48**, 1687 (1993); J. Kempe, Contemp. Phys. **44**, 307 (2003).
[9] D. K. Wójcik and J. R. Dorfman, Phys. Rev. Lett. **90**, 230602 (2003); D. K. Wójcik, Int. J. Mod. Phys. B **20**, 1969 (2006).
[10] B. C. Sanders, S. D. Bartlett, B. Tregenna, and P. L. Knight, Phys. Rev. A **67**, 042305 (2003).
[11] H. B. Perets *et al.*, e-print arXiv:0707.0741.
[12] W. Dür, R. Raussendorf, V. M. Kendon, and H. J. Briegel, Phys. Rev. A **66**, 052319 (2002).
[13] R. Côté *et al.*, New J. Phys. **8**, 156 (2006).
[14] O. Mülken, A. Blumen, T. Amthor, C. Giese, M. Reetz-Lamour, and M. Weidemuller, Phys. Rev. Lett. **99**, 090601 (2007).
[15] W. R. Anderson, J. R. Veale, and T. F. Gallagher, Phys. Rev. Lett. **80**, 249 (1998).
[16] G. H. Weiss, *Aspects and Applications of the Random Walk* (North-Holland, Amsterdam, 1994).
[17] J. Klafter, A. Blumen, and M. F. Shlesinger, Phys. Rev. A **35**, 3081 (1987).
[18] L. Borland and J. G. Menchero, Braz. J. Phys. **29**, 169 (1999); L. Borland, J. G. Menchero, and C. Tsallis, Phys. Rev. B **61**, 1650 (2000).
[19] I. S. Gradshteyn and I. M. Ryzhik, *Table of Integrals, Series, and Products* (Academic Press, New York, 1980).
[20] *Handbook of Mathematical Functions*, edited by M. Abramowitz and I. A. Stegun (Dover, New York, 1972).
[21] A. Rodríguez, V. A. Malyshev, G. Sierra, M. A. Martin-Delgado, J. Rodriguez-Laguna, and F. Dominguez-Adame, Phys. Rev. Lett. **90**, 027404 (2003).
[22] S. Alexander *et al.*, Rev. Mod. Phys. **53**, 175 (1981).
[23] A. J. Bray and G. J. Rodgers, Phys. Rev. B **38**, 11461 (1988).
[24] O. Mülken and A. Blumen, Phys. Rev. E **73**, 066117 (2006).
[25] C. M. Bender and S. A. Orszag, *Advanced Mathematical Methods for Scientists and Engineers* (McGraw-Hill, New York, 1978).